 CMES, vol.57, no.3, pp.225-243, 2010

Shape Memory Alloy: from Constitutive Modeling to Finite Element Analysis of Stent Deployment

F. Auricchio[1,2,3,4] **M. Conti**[1,5] **S. Morganti**[1] **and A. Reali**[1,2,3]

Abstract: The use of shape memory alloys (SMA) in an increasing number of applications in many fields of engineering, and in particular in biomedical engineering, is leading to a growing interest toward an exhaustive modeling of their macroscopic behavior in order to construct reliable simulation tools for SMA-based devices. In this paper, we review the properties of a robust three-dimensional model able to reproduce both pseudo-elastic and shape-memory effect; then we calibrate the model parameters on experimental data and, finally, we exploit the model to perform the finite element analysis of pseudo-elastic Nitinol stent deployment in a simplified atherosclerotic artery model.

Keywords: shape memory alloys (SMA), shape-memory effect, pseudo-elasticity, finite element analysis (FEA), stent deployment, experimental parameter calibration.

1 Introduction

The great and always growing interest in shape memory alloys (SMA) (cf. Duerig, Melton, Stoekel, and Wayman (1990); Gong, Duerig, Pelton, Rebelo, and Perry (2003); Roh and Lee (2008)) and in their industrial applications in many branches of engineering is deeply stimulating the research on suitable and reliable constitutive laws. As a consequence, many models able to reproduce one or both of the well-known SMA macroscopic behaviors, referred to as *pseudo-elasticity* and *shape-memory effect*, have been proposed in the literature in the last years (refer for instance to Raniecki and Lexcellent (1994); Leclercq and Lexcellent (1996); Levitas (1998); Govindjee and Miehe (2001); Levitas and Preston (2002a,b); Helm

[1] Department of Structural Mechanics, University of Pavia, Pavia, Italy.
[2] European Centre for Training and Research in Earthquake Engineering (EUCENTRE), Pavia, Italy
[3] Istituto di Matematica Applicata e Tecnologie Informatiche del CNR (IMATI), Pavia, Italy.
[4] Centro di Simulazione Numerica Avanzata (CESNA), Pavia, Italy.
[5] Institute Biomedical Technology (IBiTech), Ghent University, Ghent, Belgium.

and Haupt (2003); Bouvet, Calloch, and Lexcellent (2004); Lagoudas and Entchev (2004); Peultier, Benzineb, and Patoor (2004); Panico and Brinson (2007)). In particular, the constitutive law proposed by Souza, Mamiya, and Zouain (1998) and improved by Auricchio and Petrini (2004a) seems to be attractive. Developed within the theory of irreversible thermodynamics, this model is in fact able to describe both pseudo-elasticity and shape-memory effect and the corresponding solution algorithm is simple and robust as it is based on a plasticity-like return map procedure. The robustness of such a model makes it particularly suitable for implementation within finite element codes, allowing in this way the simulation of the behavior of complex SMA devices (Auricchio, Petrini, Pietrabissa, and Sacco, 2003). In this paper we review the properties of this model and we report some results from the simulations of SMA-based devices, such as pseudo-elastic stents.

2 3D SMA Phenomenological Model

In this first part of the paper we present and discuss in detail the 3D phenomenological model for SMA as reported in Auricchio and Petrini (2004a,b) following Souza, Mamiya, and Zouain (1998).

The model assumes the total strain $\boldsymbol{\varepsilon}$ and the absolute temperature T as control variables, the transformation strain $\mathbf{e}^{tr}$ as internal one. The second-order tensor $\mathbf{e}^{tr}$ describes the strain associated to the transformation between the two solid phases referred to as martensite and austenite. Here, this quantity should have a fully reversible evolution and should be completely recovered when unloading to a zero stress state. Moreover, we require that

$$\|\mathbf{e}^{tr}\| \leq \varepsilon_L,$$

where $\|\cdot\|$ is the usual Euclidean norm and ε_L is a material parameter corresponding to the maximum transformation strain reached at the end of the transformation during a uniaxial test. Moreover, $\mathbf{e}^{tr}$ is assumed to be deviatoric, since, following experimental evidences, SMA phase transformations take place under (nearly) isochoric conditions.

Assuming a small strain regime, justified by the fact that the approximation of large deformations and small strains is valid for several applications, the following standard additive decomposition can be considered

$$\boldsymbol{\varepsilon} = \frac{\theta}{3}\mathbf{1} + \mathbf{e},$$

where $\theta = \mathrm{tr}(\boldsymbol{\varepsilon})$ and $\mathbf{e}$ are respectively the volumetric and the deviatoric part of the total strain $\boldsymbol{\varepsilon}$, while $\mathbf{1}$ is the second-order identity tensor. The free energy density

function Ψ for a polycrystalline SMA material is then expressed as the convex potential

$$\begin{aligned}\Psi(\theta,\mathbf{e},T,\mathbf{e}^{tr}) &= \frac{1}{2}K\theta^2 + G\|\mathbf{e}-\mathbf{e}^{tr}\|^2 - 3\alpha K\theta(T-T_0) + \beta\langle T-T^*\rangle\|\mathbf{e}^{tr}\| + \\ &+\frac{1}{2}h\|\mathbf{e}^{tr}\|^2 + (u_0 - T\eta_0) + c\left[T - T_0 - T\log\left(\frac{T}{T_0}\right)\right] + \mathscr{I}_{\varepsilon_L}(\mathbf{e}^{tr}),\end{aligned}$$

where K and G are respectively the bulk and the shear modulus, α is the thermal expansion coefficient, β is a material parameter related to the dependence of the critical stress on the temperature, T^* is the temperature below which only martensite phase is stable, h defines the hardening of the phase transformation, c is the heat capacity, and u_0, η_0 and T_0 are, respectively, the internal energy, the entropy and the temperature at the reference state. Moreover, we make use of the indicator function

$$\mathscr{I}_{\varepsilon_L}(\mathbf{e}^{tr}) = \begin{cases} 0 & \text{if } \|\mathbf{e}^{tr}\| \le \varepsilon_L \\ +\infty & \text{otherwise,} \end{cases}$$

in order to satisfy the transformation strain constraint ($\|\mathbf{e}^{tr}\| \le \varepsilon_L$); we also introduce the positive part function $\langle\cdot\rangle$, defined as

$$\langle a\rangle = \begin{cases} a & \text{if } a > 0 \\ 0 & \text{otherwise.} \end{cases}$$

We remark that, since we use only a single internal variable to describe phase transformations, it is possible to distinguish between a generic parent phase (not associated to any macroscopic strain) and a generic product phase (associated to a macroscopic strain). Accordingly, the model does not distinguish between the austenite and the twinned martensite, as both these phases do not produce macroscopic strain.

We furthermore highlight that, for the sake of simplicity, the present model does not reflect the differences existing between the austenite and the martensite elastic properties (see Auricchio, Reali, and Stefanelli (2009) for a way to include this in the model).

Starting from the free energy function Ψ and following standard arguments, we can

derive the constitutive equations

$$\begin{cases} p = \dfrac{\partial \Psi}{\partial \theta} = K\left[\theta - 3\alpha(T-T_0)\right], \\ \mathbf{s} = \dfrac{\partial \Psi}{\partial \mathbf{e}} = 2G(\mathbf{e}-\mathbf{e}^{tr}), \\ \eta = -\dfrac{\partial \Psi}{\partial T} = \eta_0 + 3\alpha K\theta - \beta\|\mathbf{e}^{tr}\|\dfrac{\langle T-T^*\rangle}{|T-T^*|} + c\log\left(\dfrac{T}{T_0}\right), \\ \mathbf{X} = -\dfrac{\partial \Psi}{\partial \mathbf{e}^{tr}} = \mathbf{s} - \beta\langle T-T^*\rangle\dfrac{\mathbf{e}^{tr}}{\|\mathbf{e}^{tr}\|} - h\mathbf{e}^{tr} - \gamma\dfrac{\mathbf{e}^{tr}}{\|\mathbf{e}^{tr}\|}, \end{cases} \tag{1}$$

where $p = \mathrm{tr}(\sigma)/3$ and $\mathbf{s}$ are respectively the volumetric and the deviatoric part of the stress σ, $\mathbf{X}$ is a thermodynamic stress-like quantity associated to the transformation strain $\mathbf{e}^{tr}$, and η is the entropy. The variable γ results from the indicator function subdifferential $\partial \mathscr{I}_{\varepsilon_L}(\mathbf{e}^{tr})$ and it is defined such that

$$\begin{cases} \gamma = 0 & if\ \|\mathbf{e}^{tr}\| < \varepsilon_L, \\ \gamma \geq 0 & if\ \|\mathbf{e}^{tr}\| = \varepsilon_L, \end{cases}$$

yielding $\partial \mathscr{I}_{\varepsilon_L}(\mathbf{e}^{tr}) = \gamma \mathbf{e}^{tr}/\|\mathbf{e}^{tr}\|$.

To describe phase transformation and inelasticity evolution, we choose a Mises-type limit function F defined as

$$F(\mathbf{X}) = \|\mathbf{X}\| - R, \tag{2}$$

where R is the radius of the elastic domain in the deviatoric space. We remark that this simple choice for the limit function is not able to reproduce asymmetric (e.g., between tension and compression) behaviors. However, a strategy to include in the proposed model tension-compression asymmetries (as exhibited by some SMA materials) can be found in Auricchio, Reali, and Stefanelli (2009).

Considering an associative framework, the flow rule for the internal variable takes the form

$$\dot{\mathbf{e}}^{tr} = \dot{\zeta}\frac{\partial F}{\partial \mathbf{X}} = \dot{\zeta}\frac{\mathbf{X}}{\|\mathbf{X}\|}, \tag{3}$$

where $\dot{\zeta}$ is the consistency parameter.

The model is then completed by the classical Kuhn-Tucker conditions

$$\begin{cases} \dot{\zeta} \geq 0, \\ F \leq 0, \\ \dot{\zeta}F = 0. \end{cases} \tag{4}$$

Following classical arguments (Lemaitre and Chaboche, 1990), we can also compute the evolution of the current internal energy u, using the first principle of thermodynamics, as

$$\dot{u} = \dot{\Psi} + T\dot{\eta} + \dot{T}\eta = \sigma : \dot{\varepsilon} + r - \nabla \cdot \mathbf{q}, \tag{5}$$

being r and $\mathbf{q}$, respectively, the heat source and flux vector.

3 Time-Discrete Frame and Solution Algorithm

In order to solve the non-linear problem described in the previous section, from a computational point of view, we consider an implicit time-discrete strain-driven problem. Accordingly, we introduce a subdivision of the time interval of interest $[0, t_f]$ and solve the evolution problem over the generic interval $[t_n, t_{n+1}]$ with $t_{n+1} > t_n$.
Note that in the following, for the sake of notation simplicity, we drop the subindex $n+1$ for all the variables computed at time $t = t_{n+1}$.
Assumed to be given the solution at time t_n and the value of the total strain at time t, the implicit backward Euler scheme is employed to integrate the model rate equations.
From now on, we limit the discussion only to problems for which we assume the temperature constant and given during each time-step. Accordingly, we are required to solve only the mechanical part of the model, assuming at every instant a given temperature which may be variable in time and space during the analysis but not within the single time-step.

The time-discrete counterpart of the constitutive model is:

$$\begin{aligned}
&p = K[\theta - 3\alpha(T - T_0)] \\
&\mathbf{s} = 2G(\mathbf{e} - \mathbf{e}^{tr}) \\
&\mathbf{X} = \mathbf{s} - \beta\langle T - T^* \rangle \frac{\mathbf{e}^{tr}}{\|\mathbf{e}^{tr}\|} - h\mathbf{e}^{tr} - \gamma \frac{\mathbf{e}^{tr}}{\|\mathbf{e}^{tr}\|} \\
&\gamma \geq 0 \\
&\mathbf{e}^{tr} = \mathbf{e}_n^{tr} + \Delta\zeta \frac{\mathbf{X}}{\|\mathbf{X}\|} \\
&\|\mathbf{e}^{tr}\| \leq \varepsilon_L \\
&F(\mathbf{X}) = \|\mathbf{X}\| - R \leq 0 \\
&\Delta\zeta \geq 0, \quad \Delta\zeta F(\mathbf{X}) = 0
\end{aligned} \tag{6}$$

where $\Delta\zeta = (\zeta - \zeta_n)$ is the consistency parameter time-integrated over the interval $[t_n, t]$.

From a computational standpoint, the time-discrete model as presented in equations (6) shows a major problem, since the transformation stress $\mathbf{X}$ depends on the derivative of the transformation strain which can be null, making the derivative undefined. To overcome this difficulty, different approaches can be followed (Auricchio and Petrini, 2002; Helm and Haupt, 2003). Therefore, following Auricchio, Reali, and Stefanelli (2007), we propose to substitute, in the free energy function, the Euclidean norm $\|\mathbf{e}^{tr}\|$ with a regularized norm $\overline{\|\mathbf{e}^{tr}\|}$, defined as:

$$\overline{\|\mathbf{e}^{tr}\|} = \sqrt{\|\mathbf{e}^{tr}\|^2 + \delta} - \sqrt{\delta}$$

where δ is a (small) positive user-defined parameter which controls the smoothness of the regularized norm (with typical values in the order for 10^{-8}). The quantity $\overline{\|\mathbf{e}^{tr}\|}$ is always differentiable, even for $\|\mathbf{e}^{tr}\| = \mathbf{0}$.

Stress is then derived from strain by means of an elastic-predictor inelastic-corrector *return map* as in classical plasticity problems (Simo and Hughes, 1998). An elastic trial state is evaluated for frozen internal variables and a trial value of the limit function is computed in order to check the admissibility of the trial state. If the latter is not verified, the step is inelastic and the evolution equations are integrated. We solve the inelastic step with the following procedure:

- We first assume to be in an unsaturated condition (i.e., $\|\mathbf{e}^{tr}\| < \varepsilon_L$), which implies $\gamma = 0$, and rewrite equation (6) in residual form as follows:

$$\begin{aligned} &\mathbf{R}^X = \mathbf{X} - \mathbf{s}^{TR} + \beta \langle T - T^* \rangle \frac{\partial \overline{\|\mathbf{e}^{tr}\|}}{\partial \mathbf{e}^{tr}} + h\mathbf{e}^{tr}, \\ &R^{\Delta\zeta} = \|\mathbf{X}\| - R = 0. \end{aligned} \tag{7}$$

  We then solve the seven non-linear scalar equations above with a Newton-Raphson method to find the seven scalar unknowns, constituted by the six components of $\mathbf{X}$ and $\Delta\zeta$.

- If the above solution is not admissible (i.e., $\|\mathbf{e}^{tr}\| > \varepsilon_L$), we assume to be in a saturated condition (i.e., $\|\mathbf{e}^{tr}\| = \varepsilon_L$), which implies $\gamma > 0$, and rewrite equation (6) in residual form as follows:

$$\begin{aligned} &\mathbf{R}^X = \mathbf{X} - \mathbf{s}^{TR} + \beta \langle T - T^* \rangle \frac{\partial \overline{\|\mathbf{e}^{tr}\|}}{\partial \mathbf{e}^{tr}} + h\mathbf{e}^{tr} + \gamma \frac{\mathbf{e}^{tr}}{\|\mathbf{e}^{tr}\|}, \\ &R^{\Delta\zeta} = \|\mathbf{X}\| - R = 0, \\ &R^{\gamma} = \|\mathbf{e}^{tr}\| - \varepsilon_L = 0. \end{aligned} \tag{8}$$

  We then solve the eight non-linear scalar equations above with a Newton-Raphson method to find the eight scalar unknowns, constituted by the six components of $\mathbf{X}$, $\Delta\zeta$, and γ.

4 Experimental Calibration of Model Parameters

In this section we discuss how the present model is particularly suited for the calibration of its parameters using experimental data typical of SMA materials for actuators and other shape memory devices. In fact, the identification of the material parameters is easily achieved through a comparison between two thermal cycling tests at constant stress, in a proportional uniaxial setting, as described by Auricchio, Coda, Reali, and Urbano (2009). We remark that the proposed calibration procedure is based on proportional uniaxial experiments because these are the data typically available from the SMA producers. However, the model capabilities of capturing SMA behavior under multi-axial non-proportional loading conditions is discussed, e.g., in Arghavani, Auricchio, Naghdabadi, Reali, and Sohrabpour (2010).

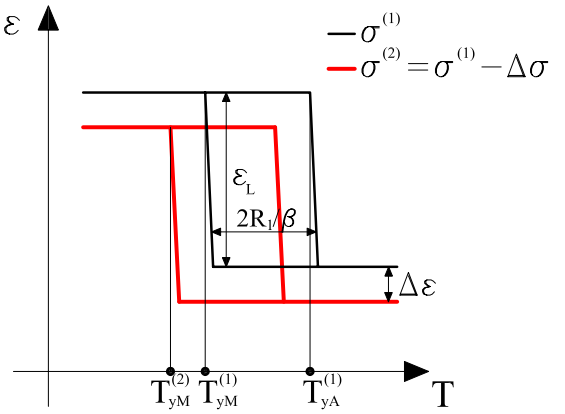

Figure 1: Two strain-temperature curves at two constant stresses $\sigma^{(1)} > \sigma^{(2)}$.

In particular, as shown in Figure 1, ε_L is immediately obtained, while E and β can be computed, using their definition, respectively as

$$E = \frac{\Delta\sigma}{\Delta\varepsilon} \quad \text{and} \quad \beta = \frac{\Delta\sigma}{\Delta T},$$

with $\Delta T = T_{yM}^{(1)} - T_{yM}^{(2)}$ and $\Delta\sigma = \sigma^{(1)} - \sigma^{(2)}$. Then, it is possible to compute R knowing that the hysteresis width is $(T_{yA}^{(1)} - T_{yM}^{(1)}) = 2R/\beta$. This is obtained subtracting the two following equations (deriving from $F = |X| - R = 0$)

$$\begin{cases} \sigma - \beta(T_{yM} - T^*) = R, \\ \sigma - \beta(T_{yA} - T^*) = -R. \end{cases}$$

Moreover, starting from $\frac{\partial \sigma}{\partial \varepsilon} = \frac{Eh}{E+h}$ and considering the dependence of the stress on temperature $\left(\frac{\partial \sigma}{\partial \varepsilon} = \frac{\partial \sigma}{\partial T} \frac{\partial T}{\partial \varepsilon} = \beta \frac{\partial T}{\partial \varepsilon} \right)$, with simple computations it can be found that

$$h = \frac{1}{\frac{1}{\beta} \frac{\partial \varepsilon}{\partial T} - \frac{1}{E}}.$$

Finally, to compute T^*, the following expression, directly derived from $\sigma^{(1)} - \beta(T_{yM}^{(1)} - T^*) = R$, can be used

$$T^* = T_{yM}^{(1)} + \frac{R - \sigma^{(1)}}{\beta}.$$

The material parameters employed in the following are obtained, with the procedure described above, from $\varepsilon - T$ curves referred to thermal cycling tests at 400 MPa and 450 MPa (Figure 2) taken from the experimental data produced within the activities of Roundrobin (2009) (see Auricchio, Morganti, and Reali (2009)).

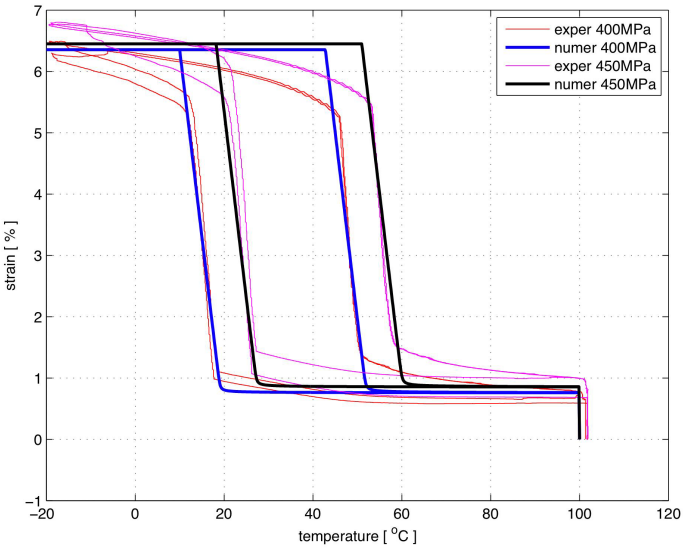

Figure 2: Strain-temperature experimental and numerical curves at 400MPa and 450 MPa used for the parameter identification.

In Table 1 we show the obtained material parameters (already reported to a 3D setting), which we will use for the numerical simulations in the next section.

Table 1: Material parameters.

E	53000 MPa
ν	0.33
h	1000 MPa
β	6.1 MPa/°C
T^*	-30 °C
R	100 MPa
ε_L	5.6 %

5 FEA of Pseudo-Elastic Stent Deploymemt

In this section, we provide an example of the use of the proposed constitutive model for applicative purpose: the finite element analysis (FEA) investigation of the mechanical behavior of two different pseudo-elastic stent designs and of their relative impact on the same vessel. We first briefly introduce the device under investigation and we then focus on the performed FEA exploiting the numerical implementation of the SMA model.

Cardiovascular diseases (CVD) are the main cause of death in Europe having every year a huge impact on economical and social costs (Petersen, Peto, Rayner, Leal, Luengo-Fernandez, and Gray, 2005). CVD are often related to atherosclerosis, a degeneration of the vessel wall narrowing the lumen and consequently reducing or blocking the blood flow.

The deployment of an intravascular tubular prosthesis, called stent, has become a common and widely-used treatment for atherosclerotic coronary arteries and the current trend is to apply this technique to atherosclerotic peripheral vessels such as carotid artery (CA) or superficial femoral artery (SFA). Peripheral Nitinol stents are usually obtained by laser-cutting a small diameter (e.g., 2 mm) tube and then setting both the shape and the material properties by thermo-mechanical treatments; after appropriate surface treatments, the final product of the stent manufacturing is crimped within a delivery system, which is mainly composed by a low profile catheter. During the medical procedure, the stent is driven to the stenosis and, when the target is reached, the constraints of the delivery system are released and the stent deploys due to the pseudo-elastic effect. The stent deployment is usually anticipated by an angioplasty (mechanical enlargement of the plaque by balloon inflation). Besides the deployment mechanism, the Nitinol pseudo-elastic effect is

also very important to allow in-service large recoverable deformation of the stent, especially in peripheral vessels characterized by tortuous anatomy and significant loading due to the body kinematics (Smouse, Nikanorov, and LaFlash, 2005). Although Nitinol stents accomplish both technical and biomechanical requirements (i.e., flexibility, kink resistance, low delivery profile, etc.), it has been observed that many of these stents implanted in peripheral vessels fail (Allie, Hebert, and Walker, 2004; Scheinert, Scheinert, Sax, Piorkowski, Bräunlich, Ulrich, Biamino, and Schmidt, 2004).

Currently, several peripheral stent designs, with different intrinsic mechanically features (Nikanorov, Smouse, Osman, Bialas, Shrivastava, and Schwartz, 2004), are available on a dedicated, fast-growing market. They, on one hand, are enlarging the available interventional options but, on the other hand, are complicating the standardization of the treatment strategy (Stockx, 2006).

Finite element analysis has shown to be a very useful tool in the investigation and optimization of stent design (Auricchio, Di Loreto, and Sacco, 2000; De Beule, 2009), also providing novel insights on fatigue/fracture mechanics (Marrey, Burgermeister, Grishber, and Ritchie, 2006).

An accurate simulation of peripheral stenting should face the following issues:

- accurate modeling of both peripheral artery and stent design;
- simulation of stent manufacturing process;
- assessment and implementation of stent material properties;
- assessment and implementation of atherosclerotic vessel material properties;
- accurate modeling of stent deployment;
- loading induced by pulsatile blood flow and vessel kinematics.

Since our simulation mainly focuses on the third item, we introduce the following simplifications to reduce the computational cost:

- the artery is modeled as a straight cylinder;
- the plaque is modeled as a cylinder (symmetric plaque);
- the anisotropic behavior of vessel and plaque tissue is neglected;
- only a small portion of stent is taken into account;

- the blood pressure is applied as a uniform pressure on the inner wall of the atherosclerotic vessel;
- pre- or post-stenting angioplasty are not taken into account.

Examples of simulations about Nitinol stent implants addressing accurate vessel modeling and loading conditions can be found in the literature (Conti, Auricchio, De Beule, and Verhegghe, 2009; Rebelo, Fu, and Lawrenchuk, 2009; Wu, Qi, Liu, Yang, and Wang, 2007); the present study focuses more on the assessment and implementation of the stent material behavior.

We consider the two following different stent designs (see Figure 3(a,b)):

- Stent A: The model reproduces a portion of an open-cell[1] carotid stent, in particular, the ACCULINK stent (Abbott, Illinois, USA);
- Stent B: The model reproduces a portion of a closed-cell carotid stent, in particular, the XACT stent (Abbott, Illinois, USA);

For each stent, we perform a small-strain and large-rotation analysis with the FEM commercial code ABAQUS/STD (version 6.8 - Dassault Systémes Simulia Corp., Providence, RI, USA) using the option "nlgeom" (Abaqus Theory Manual, Hughes and Winget (1980)). in each FEA, the stent model is associated with other three parts (see Figure 3(c,d)):

1. the artery;
2. the atherosclerotic plaque;
3. the catheter.

Both stents are considered in open configuration and the main stent geometrical features are reported in Table 2.

Stent A is discretized by means of 40068 3D linear hexahedral (C3D8) elements corresponding to 66600 nodes, while stent B is discretized by means of 54432 elements corresponding to 89820 nodes.
Both stents are assumed to be manufactured in Nitinol and their peculiar constitutive behavior is described using an ad-hoc developed algorithm, implementing the

[1] *open* and *closed* cell design: a classification of peripheral stents based on the number and arrangement of bridge connectors; in *closed* cell stents, adjacent ring segments are connected at every possible junction; in *open* cell stents not all of the junction points are interconnected.

Table 2: Geometrical features of the considered stent designs.

	Stent *A*	Stent *B*
Outer diameter	8.4 mm	8.01 mm
Length	10.20 mm	10.20 mm
Strut thickness	0.124 mm	0.182 mm

model discussed in Section 2 into the ABAQUS/STD code through a user material subroutine (UMAT). We assume that: i) the stents have the same Nitinol material properties; ii) the relative material parameters are those identified in Section 4 and reported in Table 1; the working temperature is set to $37^{\circ}C$, and consequently the material exhibits the pseudo-elastic behavior shown in Figure 4 (left).
We consider a simplified model of atherosclerotic artery with a reduced level of stenosis since the generation of more accurate vessel model requires a discussion which further from the aim of the present study. Consequently we model the artery as a cylinder having a length of 12 mm, an internal diameter of 6 mm and a thickness of 0.7 mm. The model is discretized by means of 11520 3D linear hexahedral hybrid with constant pressure (C3D8H), elements corresponding to 15520 nodes. We model the plaque as a cylinder (symmetric plaque) with a length of 4 mm and an internal diameter of 4.8 mm, corresponding to a stenosis of 20%. To describe the mechanical behavior of both artery and plaque, we use the hyperelastic isotropic material model proposed by Lally, Dolan, and Prendergast (2005); in Figure 4 (right) the stress-strain curves of the adopted material models are reported. The catheter has an initial diameter of 8.4 mm and is used to force the radial deformation of the stent during the simulation; the catheter model is discretized by 3510 3D quadrilateral surface elements with reduced integration (SFM3D4R) corresponding to 3600 nodes.

The simulation is defined by the following two steps:

1. crimping of the stent and vessel inflation by a physiological pressure (100 mmHg);

2. stent expansion in the vessel.

In the first step, we impose a radial displacement of 3.2 mm to the whole catheter in order to crimp the stent; only the contact between the outer stent surface and the inner catheter surface is activated; moreover the nodes lying at the proximal end of the stent were fixed in circumferential and longitudinal direction. In the second step, we gradually release the catheter boundary conditions allowing its re-expansion and thus the stent deployment; during this step, we activate also the

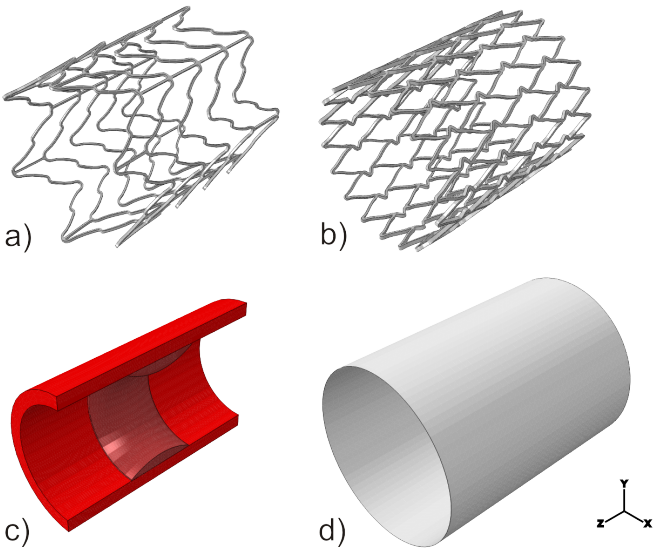

Figure 3: Geometry of the 3D models: a) Stent *A* in the expanded configuration; b) Stent *B* in the expanded configuration; c) cut view (x=0) of artery (light red) and plaque (dark red); d) catheter.

contact between the outer surface of the stent and the inner surface of the vessel. All the nodes lying at the distal and proximal vessel ends have been fixed in circumferential and longitudinal direction during the whole analysis.
We analyze the results focusing in particular on the following issues: i) the vessel injury induced by stent deployment (evaluating the von Mises stress distribution in the tissue); ii) the in-service loading state of the stent (evaluating the von Mises stress distribution in the structure). Figure 5 depicts the results of the simulation highlighting the deformed configuration of both the stents and of the vessel after the deployment; both stents are able to enlarge the lumen having a similar performance; in particular minimum post-stenting vessel diameter is 5.53 mm using stent *A* and 6 mm using stent *B*.

As highlighted in Figure 6, showing the von Mises stress distribution in post-stenting vessel, stent *B* induces a major stress level when compared to stent *A*, especially in the plaque.
Figure 7 shows the von Mises stress distribution along the stent structure: stent *B*, with its closed cell design, experiences a more extended distribution of the higher

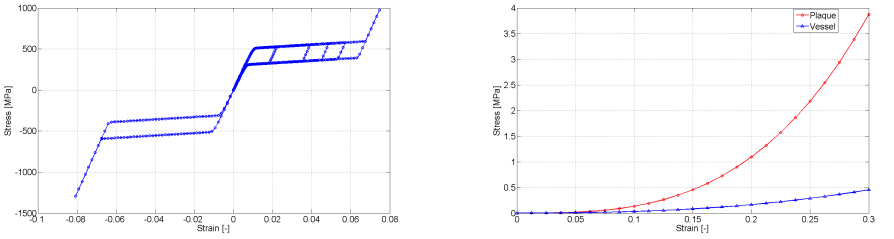

Figure 4: Nitinol pseudo-elastic behavior based on a uniaxial test (left) and hyper-elastic behavior of vessel and plaque tissues based on uniaxial tests (right).

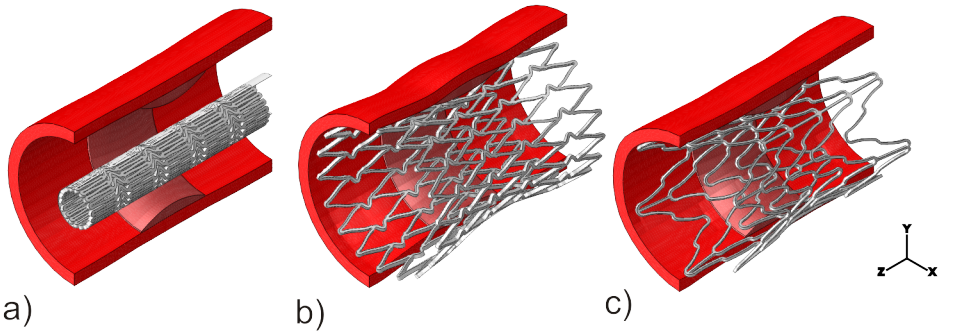

Figure 5: Results of the simulations: a) Stent B in the crimped configuration; b) Stent B deployed in the vessel; c) Stent A deployed in the vessel.

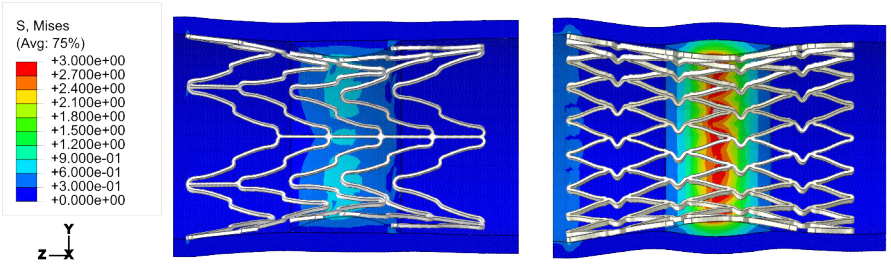

Figure 6: Von Mises stress distribution [MPa] in the post-stenting vessel: stent *A* (left); stent *B* (right).

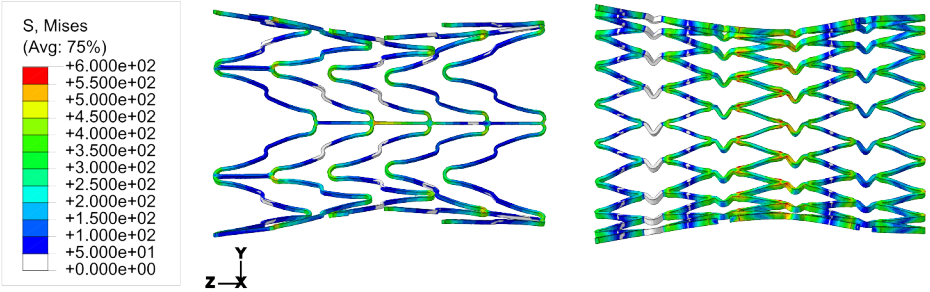

Figure 7: Von Mises stress distribution [MPa] in the stent structures: stent *A* (left); stent *B* (right).

stress level when compared to stent *A*. In fact, the plaque induces a localized deformation at the center of the structure which can be prone to fracture as highlighted in clinical practice (Ling, Mwipatayi, Gandhi, and Sieunarine, 2005).
Although the discussed simplifying assumptions, the study discussed in the present section shows how the numerical implementation of the SMA constitutive model presented in Section 2 can be easily exploited within FEM codes for applicative purpose such as the comparison of two different stent designs. Moreover, given the strong dependency of SMA properties from the alloy composition and thermomechanical treatment, the simple model parameter calibration procedure discussed in the previous section represents an important added-value in view of FEA applications.

6 Conclusions

In this paper we moved from an analytical description of a three-dimensional phenomenological SMA constitutive model toward its application within a finite element code for the simulation of pseudo-elastic stent deployment, investigating both the time-discrete frame and the experimental calibration of model parameters.
The SMA constitutive equations, herein presented and developed within the theory of irreversible thermodynamics, are able to reproduce both the pseudo-elastic effect and the shape-memory effect and the corresponding solution algorithm is simple and robust. We also illustrated a procedure to experimentally calibrate model parameters starting from strain-temperature experimental curves at different constant stresses.
Taking advantage of the model robustness, we then implemented it within the commercial finite element code Abaqus, aiming at the simulation and comparison of the deployment behavior of two different stent designs. Despite the adopted simplified assumptions, the obtained results are interesting and show that the proposed approach can be successfully applied to perform numerical simulations which can support the design of SMA-based biomedical devices, like stents. To pursue this goal, more work along this research line is in order and will be the subject of future communications.

Acknowledgement: The authors were partially supported by the Cariplo Foundation through the project number n.2009.2822; by the Ministero dell'Istruzione, dell'Università e della Ricerca through the project n. 2008MRKXLX; and by the European Research Council through the Starting Independent Research Grant "BioSMA: Mathematics for Shape Memory Technologies in Biomechanics". This support is gratefully acknowledged.

References

Allie, D.; Hebert, C.; Walker, C. (2004): Nitinol Stent Fractures in the SFA. *Endovascular Today*, pp. 22–34.

Arghavani, J.; Auricchio, F.; Naghdabadi, R.; Reali, A.; Sohrabpour, S. (2010): A 3-d phenomenological constitutive model for shape memory alloys under multiaxial loadings. *International Journal of Plasticity,* doi:10.1016/j.ijplas.2009.12.003.

Auricchio, F.; Coda, A.; Reali, A.; Urbano, M. (2009): SMA Numerical Modeling versus Experimental Results: Parameter Identification and Model Prediction Capabilities. *Journal of Materials Engineering and Performance*, vol. 18, pp. 649–654.

Auricchio, F.; Di Loreto, M.; Sacco, E. (2000): Finite Element Analysis of a Stenotic Artery Revascularization through Stent Insertion. *Computational Methods in Biomechanics and Biomedical Engineering*, vol. 0, pp. 1–15.

Auricchio, F.; Morganti, S.; Reali, A. (2009): SMA Numerical Modeling versus Experimental Results. In *ESOMAT09 Proceedings*.

Auricchio, F.; Petrini, L. (2002): Improvements and Algorithmical Considerations on a Recent Three-dimensional Model Describing Stress-induced Solid Phase Transformations. *International Journal for Numerical Methods in Engineering*, vol. 55, pp. 1255–1284.

Auricchio, F.; Petrini, L. (2004a): A three-dimensional Model Describing Stress-temperature Induced Solid Phase Transformations. Part I: Solution Algorithm and Boundary Value Problems. *International Journal for Numerical Methods in Engineering*, vol. 61, pp. 807–836.

Auricchio, F.; Petrini, L. (2004b): A Three-dimensional Model Describing Stress-temperature Induced Solid Phase Transformations. Part II: Thermomechanical Coupling and Hybrid Composite Applications. *International Journal for Numerical Methods in Engineering*, vol. 61, pp. 716–737.

Auricchio, F.; Petrini, L.; Pietrabissa, R.; Sacco, E. (2003): Numerical modeling of shape-memory alloys in orthodontics. *CMES: Computer Modeling in Engineering & Sciences*, vol. 4, pp. 365–380.

Auricchio, F.; Reali, A.; Stefanelli, U. (2007): A Three-dimensional Model Describing Stress-induced Solid Phase Transformation with Permanent Inelasticity . *International Journal of Plasticity*, vol. 23, pp. 207–226.

Auricchio, F.; Reali, A.; Stefanelli, U. (2009): A Macroscopic 1D Model for Shape Memory Alloys Including Asymmetric Behaviors and Transformation-dependent Elastic Properties . *Computational Methods in Applied Mechanics and Engineering*, vol. 198, pp. 1631–1637.

Bouvet, C.; Calloch, S.; Lexcellent, C. (2004): A Phenomenological Model for Pseudoelasticity of Shape Memory Alloys under Multiaxial Proportional and Nonproportional Loadings. *European Journal of Mechanics A/Solids*, vol. 23, pp. 37–61.

Conti, M.; Auricchio, F.; De Beule, M.; Verhegghe, B. (2009): Numerical Simulation of Nitinol Peripheral Stents: from Laser-cutting to Deployment in a Patient Specific Anatomy. In *ESOMAT09 Proceedings*.

De Beule, M. (2009): *Biomechanical Modeling of Stents: Survey 1997-2007 in Advances in Biomedical Engineering*. Edited by P. Verdonck (Elsevier).

Duerig, T.; Melton, K.; Stoekel, D.; Wayman, C. (1990): *Engineering Aspects of Shape Memory Alloys*. Butterworth-Heinemann.

Gong, X.; Duerig, T.; Pelton, A.; Rebelo, N.; Perry, K. (2003): Finite element analysis and experimental evaluation of superelastic nitinol stents. In *Proceedings of the International Conference on Shape Memory and Superelastic Technology Conference - SMST*.

Govindjee, S.; Miehe, C. (2001): A Multi-Variant Martensitic Phase Transformation Model: Formulation and Numerical Implementation. *Computational Methods in Applied Mechanics and Engineering*, vol. 191, pp. 215–238.

Helm, D.; Haupt, P. (2003): Shape Memory Behaviour: Modelling within Continuum Thermomechanics. *International Journal of Solids and Structures*, vol. 40, pp. 827–849.

Hughes, T.; Winget, J. (1980): Finite Rotation Effects in Numerical Integration of Rate Constitutive Equations Arising in Large Deformation Analysis. *International Journal for Numerical Methods in Engineering*, vol. 15, pp. 1862–1867.

Lagoudas, D.; Entchev, P. (2004): Modeling of Transformation-induced Plasticity and its Effect on the Behavior of Porous Shape Memory Alloys. Part I: Constitutive Model for Fully Dense SMAs. *Mechanics of Materials*, vol. 36, pp. 865–892.

Lally, C.; Dolan, F.; Prendergast, P. (2005): Cardiovascular Stent Design and Vessel Stresses: a Finite Element Analysis. *Journal of Biomechanics*, vol. 38, pp. 1574–1581.

Leclercq, S.; Lexcellent, C. (1996): A General Macroscopic Description of the Thermomechanical Behavior of Shape Memory Alloy. *Journal of the Mechanics and Physics of Solids*, vol. 44, pp. 953–980.

Lemaitre, J.; Chaboche, J. (1990): *Mechanics of Solid Materials*. Cambridge University Press.

Levitas, V. (1998): Thermomechanical Theory of Martensitic Phase Transformations in Inelastic Materials. *International Journal of Solids and Structures*, vol. 35, pp. 889–940.

Levitas, V. I.; Preston, D. L. (2002): Three-dimensional Landau Theory for Multivariant Stress-induced Martensitic Phase Transformations. I. Austenite↔ Martensite. *Physical Review B*, vol. 66, no. 13, pp. 134206:1–9.

Levitas, V. I.; Preston, D. L. (2002): Three-dimensional Landau Theory for Multivariant Stress-induced Martensitic Phase Transformations. II. Multivariant Phase Transformations and Stress Space Analysis. *Physical Review B*, vol. 66, no. 13, pp. 134207:1–15.

Ling, A.; Mwipatayi, P.; Gandhi, T.; Sieunarine, K. (2005): Stenting for Carotid Artery Stenosis: Fractures, Proposed Etiology and the Need for Surveillance. *Journal of Vascular Surgery*, vol. 47, pp. 1220–6.

Marrey, R. V.; Burgermeister, R.; Grishber, R.; Ritchie, R. (2006): Fatigue and Life Prediction for Cobalt-chromium Stents: a Fracture Mechanics Analysis. *Biomaterials*, vol. 27, pp. 1988–2000.

Nikanorov, A.; Smouse, H.; Osman, K.; Bialas, M.; Shrivastava, S.; Schwartz, B. (2004): Fracture of Self-expanding Nitinol Stents Stressed in Vitro under Simulated Intravascular Conditions. *Journal of the American College of Cardiology*, vol. 48, pp. 435–40.

Panico, M.; Brinson, L. (2007): A Three-dimensional Phenomenological Model for Martensite Reorientation in Shape Memory Alloys. *Journal of the Mechanics and Physics of Solids*, vol. 55, pp. 2491–2511.

Petersen, S.; Peto, V.; Rayner, M.; Leal, J.; Luengo-Fernandez, R.; Gray, A. (2005): *European Cardiovascular Disease Statistics*. BHF London.

Peultier, B.; Benzineb, T.; Patoor, E. (2004): Modelling of the Martensitic Phase Transformation for Finite Element Computation. *Journal de Physique IV*, vol. 115, pp. 351–359.

Raniecki, B.; Lexcellent, C. (1994): RL- models of Pseudoelasticity and their Specification for some Shape Memory Solids. *European Journal of Mechanics A/Solids*, vol. 13, pp. 21–50.

Rebelo, N.; Fu, R.; Lawrenchuk, M. (2009): Study of a Nitinol Stent Deployed into Anatomically Accurate Artery Geometry and Subjected to Realistic Service Loading. *Journal of Materials Engineering and Performance*, vol. 27, pp. doi: 10.1007/s11665–009–9375–0.

Roh, J.; Lee, I. (2008): Configuration Maintenance of Inflated Membrane Structures Using SMA Film Actuators. *CMES: Computer Modeling in Engineering & Sciences*, vol. 26, pp. 13–30.

Roundrobin (2009): Esomat S3T Roundrobin SMA modeling session. *http://esomat.fzu.cz/esomat2009/index.php/esomat/esomat2009/modelling session.*

Scheinert, D.; Scheinert, S.; Sax, J.; Piorkowski, C.; Bräunlich, S.; Ulrich, M.; Biamino, G.; Schmidt, A. (2004): Prevalence and Clinical Impact of Stent Fractures after Femoropopliteal Stenting. *Journal of the American College of Cardiology*, pp. 312–315.

Simo, J.; Hughes, T. (1998): *Computational Inelasticity*. Springer-Verlag.

Smouse, H.; Nikanorov, A.; LaFlash, D. (2005): Biomechanical Forces in the Femoropopliteal Arterial Segment What happens during extremity movement and what is the effect on stenting? *Endovascular Today*, pp. 60–66.

Souza, A.; Mamiya, E.; Zouain, N. (1998): Three-dimensional Model for Solids Undergoing Stress-induced Phase Transformations. *European Journal of Mechanics A/Solids*, vol. 17, pp. 789–806.

Stockx, L. (2006): Techniques in Carotid Artery Stenting. *European Journal of Radiology*, vol. 60, pp. 11–13.

Wu, W.; Qi, M.; Liu, X.; Yang, D.; Wang, W. (2007): Delivery and Release of Nitinol Stent in Carotid Artery and their Interactions: a Finite Element Analysis. *Journal of Biomechanics*, vol. 40, pp. 3034–3040.